Journal of Engineering Research and Reports

Volume 26, Issue 1, Page 62-78, 2024; Article no.JERR.111352
ISSN: 2582-2926

Parametric Analysis on Formability of SS304 Metal Bipolar Plate with Wave Flow Field Structure

Feng Jiahao [a*], Guo Pengyan [a], He Cunwu [a] and Liu Chengwei [a]

[a] School of Mechanical Engineering, North China University of Water Resources and Electric Power, Zhengzhou, China.

Authors' contributions

This work was carried out in collaboration among all authors. All authors read and approved the final manuscript.

Article Information

DOI: 10.9734/JERR/2024/v26i11063

Open Peer Review History:
This journal follows the Advanced Open Peer Review policy. Identity of the Reviewers, Editor(s) and additional Reviewers, peer review comments, different versions of the manuscript, comments of the editors, etc are available here: https://www.sdiarticle5.com/review-history/111352

Original Research Article

Received: 04/11/2023
Accepted: 09/01/2024
Published: 12/01/2024

ABSTRACT

The main production method of metal bipolar plate is stamping, and the size parameters of the flow field structure can not only change the performance of the fuel cell, but also affect the stamping quality of the metal bipolar plate. In the case of ensuring the performance of the fuel cell, it is necessary to study the stamping of the metal bipolar plate with different flow field structures. In the past, there were few studies on the wave flow field stamping forming. This paper analyzed the wave flow field, formulated several sets of bipolar plate structural dimension parameters, and evaluated the stamping forming quality of the reaction zone of SS304 metal bipolar plate through finite element simulation. By reducing the rib height ΔH=0.075mm in the corner part, the maximum thinning rate can be reduced from 34.833% to 24.689% and the thickness can reach 0.0753mm when the flow channel width S=1.0mm, the rib width W=1.5mm and the forming depth H=0.5mm. It provides some guidance for optimizing the structural dimension parameters of metal bipolar plates.

**Corresponding author: Email: 834451968@qq.com;*

Keywords: Metal bipolar plate; flow field; stamping forming; structural dimension.

1. INTRODUCTION

With the sharp rise in energy demand, a series of environmental and energy security problems caused by the use of a large number of fossil fuels have become more and more serious [1,2]. Proton exchange membrane fuel cell (PEMFC), as a new form of hydrogen energy utilization, has the advantages of theoretical zero emission, high power density and efficiency, relatively low operating temperature and fast start-up ability, and is considered to have the potential to replace internal combustion engine [3-7]. The development and promotion of proton exchange membrane fuel cells can reduce the use of traditional fossil fuels [8] and reduce environmental pollution. However, the road to commercialization of PEMFC fuel cells is still difficult, mainly in terms of durability, reliability and cost.

The PEMFC mainly consists of bipolar plates and membrane electrodes. According to Simon et al. [9] to the cost analysis of fuel cell vehicles, the fuel cell stack accounts for about 45% of the total system cost, and the bipolar plate accounts for a relatively large part of the stack cost. The good design of the bipolar plate runner structure determines the stability of its transmission performance and output performance [10,11].Therefore, the reasonable design of the flow field structure size can improve the battery performance, the forming quality and efficiency of the bipolar plate, reduce the cost of the bipolar plate and improve the commerciality of the fuel cell.

A large number of studies have shown that fuel cell performance can be improved and production cost can be reduced by optimizing the flow field design. However, there are still few studies on the structural design of wave flow field.Jang et al. [12] designed a spiral channel. The results show that the spiral channel can enhance the mass and heat transfer.Tsung-Chia Chen [13] designed different cross section shapes of parallel runner for micro-stamping process analysis, including trapezoid, square, semi-circle and triangle. The formability of these different cross section shapes was studied and analyzed, and it was concluded that semi-circle and triangle had the best forming effect. Zhai Hua et al. [14] tried stamping metal bipolar plates with three serpentine flow channels and found that the stress at the corner position of the serpentine flow channel was relatively concentrated, the forming quality was poor, and even the phenomenon of rupture occurred. The geometric parameters such as drawing Angle, rounding radius and rib height of corner position are optimized. The results show that it is effective to increase the rounding radius and drawing Angle at the stress concentration position. Kivanc Karacan et al. [15] combined the flow field performance with the punching quality, and found that stainless steel (SS 304) was the most suitable material for the forming process. Combined with the formability of the material and the current density of the formed bipolar plate, the best combination of depth of 0.36mm and width of 1.2mm was obtained. Zhang Lili et al. [16] simulated the double-channel serpentine flow field formed on SS304 stainless steel sheet, and studied the influence of size and process parameters on the forming quality of bipolar plate, including blank holding force and drawing bar. The results show that the wrinkling of sheet metal can be reduced by increasing the holding force properly. The setting of drawbar can make the part formed more thoroughly, if the addition of double drawbar will largely eliminate the fracture, wrinkle, under-forming and other defects. Peng et al. [17] developed a 40 trapezoidal baffle structure, when the baffle Angle is 60°, the height is 1.125mm. The net power density is increased by 90% compared to conventional runner.Xia et al. [18] proposed a novel vein flow channel. The results show that the output power of the blade channel is 8.475% higher than that of the traditional channel.Liu et al. [19] studied the cross section shape of the channel with the help of genetic algorithm and concluded that the trapezoidal shape of the channel has the best performance.According to Maharudrayya S et al. [20] the use of U-shaped parallel flow channels makes the reaction more evenly distributed.

This paper analyzes the conventional wave flow field structure, formulates several groups of bipolar plate structure size parameters, and evaluates the stamping forming quality of the reaction zone of the metal bipolar plate through Dynaform simulation, which provides certain guidance for optimizing the design of the metal bipolar plate structure size parameters.

2. THREE-DIMENSIONAL MODEL

The bipolar plate and simplified die surface used in the simulation are shown in Fig. 2. The total

size of the sheet material is 50mm×50mm, S is the width of the flow channel, W is the width of the rib, H is the depth of the flow channel, R_p is the inner rounded corner, R_d is the outer rounded corner, R_w is the radius of the flow channel corner. The sine curve characteristic of wave channel is y=Asin(ωx). In this paper, the flow channel width S, rib width W, flow channel depth H, sine curve parameters A and ω are taken as the main research parameters to analyze the influence on the forming quality of stamping.

3. SIMULATION STEP

In Dynaform, the mold is further simplified, and only the convex and concave die surfaces and the sheet material are retained. In order to save computing resources, only half of the sheet material is made. Sheet metal forming type adopts double motion forming.

3.1 Plate Mesh Division and Parameter Setting

In Fig. 3,Part Mesh is used to divide sheet metal mesh, all of which are quadrilateral mesh with a size of 0.4mm. The mesh refinement is set in the stamping process, the refinement level is 4, and the minimum size is 0.025mm. The sheet material thickness is set to 0.1mm and SS304 stainless steel is selected. The performance parameters are shown in Table 1 and the stress-strain curve is shown in Fig. 4. The material type is 37*MAT_TRANSVERSELY_ANISOTR-OPIC_ELASTIC_PLASTIC. The unit type is set to FULLY INTEGRAT-ED shell units with a number of integration points of 7.

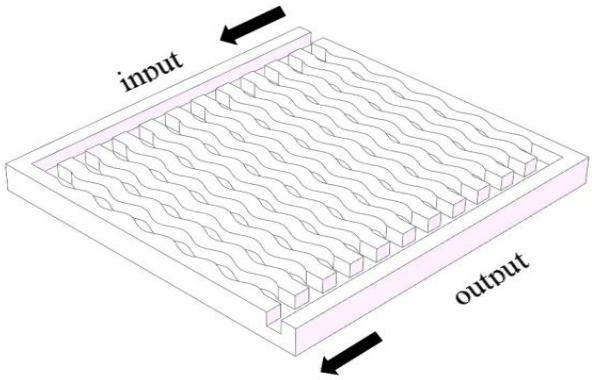

Fig. 1. Bipolar plate flow field structure

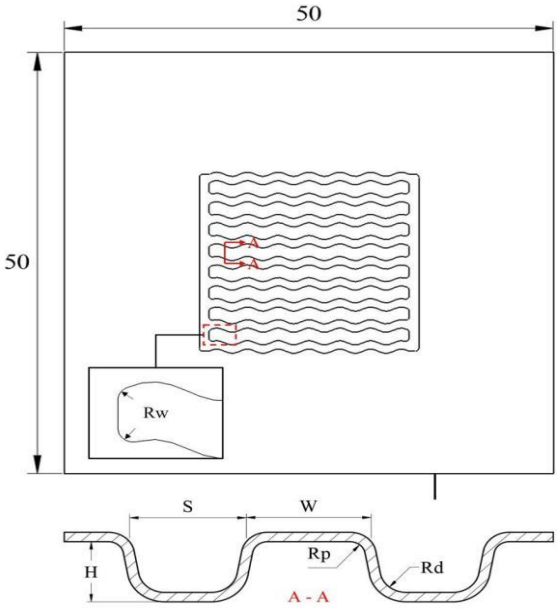

Fig. 2. Simplified model of metal bipolar plate and size of flow channel

Table 1. SS304 stainless steel material performance parameters

Density(g/cm3)	Modulus of elasticity(/MPa)	Poisson's ratio	Yield strength(MPa)	Hardening index
7.85	207000	0.28	248	0.502

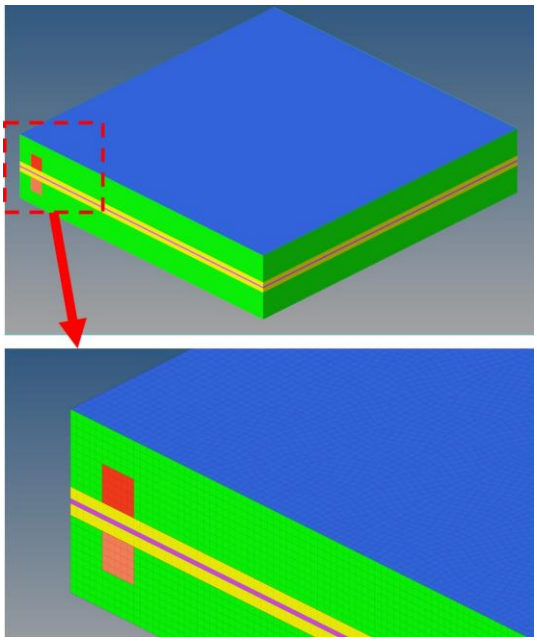

Fig. 3. Grid model

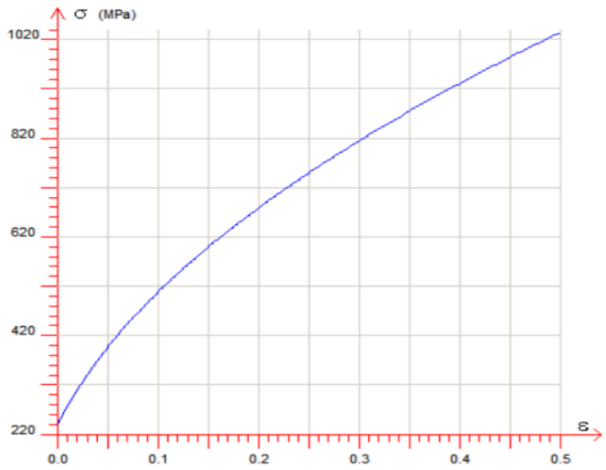

Fig. 4. Stress-strain curve

3.2 Tool Meshing and Parameter Setting

The convex and concave die of the Tool face and the flange holder are set as rigid bodies, and the Mesh is divided into the form of Tool Mesh. The mesh shape is mainly quadrilateral mesh, and the rest are triangular mesh. The maximum size is 0.4mm, the minimum size is 0.025mm, the clearance tolerance is 0.01mm, and the contact friction coefficient between the die and the plate is 0.125. The tool location information is shown in Fig. 5.

3.3 Procedure Setting

Contact mode: penalty function contact FROMING_ONE_WAY_SURFACE_TO_SURFACE, penalty function factor set to 0.15. The

closing gap is set to 0.11mm, the closing gap of the convex and concave die is 0.2mm, and the closing speed is 500mm/s. The default speed curve is adopted, The total blank holding force F_q is determined by the formula:

$$F_q = q$$

A represents the projected area of sheet blank on the blank holder ring, and q represents the unit blank holder force, and the unit blank holder force q is 3Mpa.

3. RESULTS AND DISCUSSION

4.1 Influence of Channel Width, Rib Width and Forming Depth on Forming Quality

Three channel widths and three rib widths are set, which are 0.5mm, 1.0mm, 1.5mm and 0.75mm, 1.0mm and 1.5mm respectively. The forming quality at each punching depth is obtained by simulation. The inner and outer fillet radius of the channel is a fixed value R_p=R_d=0.2mm. Because the flow channel corner radius R_w is limited by the rib width, the flow channel corner radius is uniformly set to R_w=0.35mm.

Fig. 6 shows the forming limit diagram of sheet metal at different forming depths under the parameter combination of channel width S=1.5 and rib width W=1.5. When the forming depth is gradually increased, the range and degree of severe thinning are obviously increased. With the increase of forming depth, the creasing in the corner area of the flow field edge is obviously enhanced. It can be seen that at all forming depths, the round corners of the die of the metal bipolar plate flow path will be severely thinned.

The curves of maximum thinning rate and maximum thickening rate can reflect the thinning degree and wrinkling degree of sheet metal in more detail. The left side of Fig. 8 is the maximum thinning rate of sheet metal under different parameter combinations, and the red dashed line is the maximum allowable thinning rate. The right side of Fig. 8 shows the maximum thickening rate of sheet metal. It can be seen that the maximum thickening rate of sheet metal increases with the increase of forming depth. When the width of the flow channel and the width of the rib are 1.5mm, the maximum value reaches 4.255%, and the difference between the minimum value and the flow channel width is 2.753%.

Fig. 7 shows the sheet metal forming limit diagram when the forming depth of the runner is 0.5mm. From the perspective of the change of severe thinning amount, when the width of the runner or the width of the rib is larger, the broken area is gradually eliminated, and the range of severe thinning is reduced, which mainly exists only in the corner of the runner, followed by the side wall of the runner. However, from the point of view of the change of wrinkle amount, under the same rib width or channel width setting, a larger runner width or rib width will increase the wrinkle amount at the edge corner of the flow field.

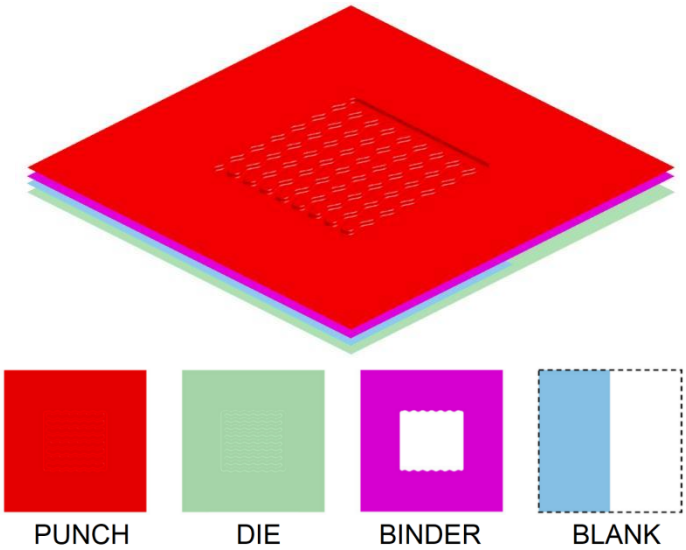

Fig. 5. Diagram of tool positioning and parts layer

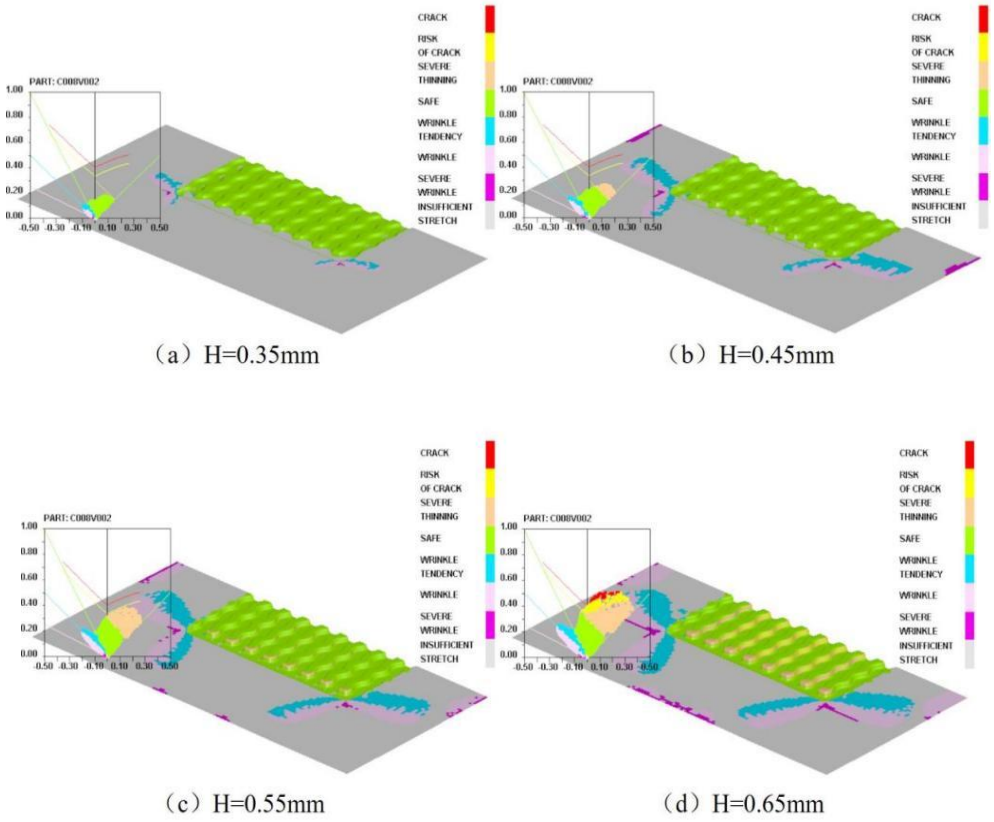

（a）H=0.35mm　　（b）H=0.45mm

（c）H=0.55mm　　（d）H=0.65mm

Fig. 6. Sheet forming limit diagram at different forming depths

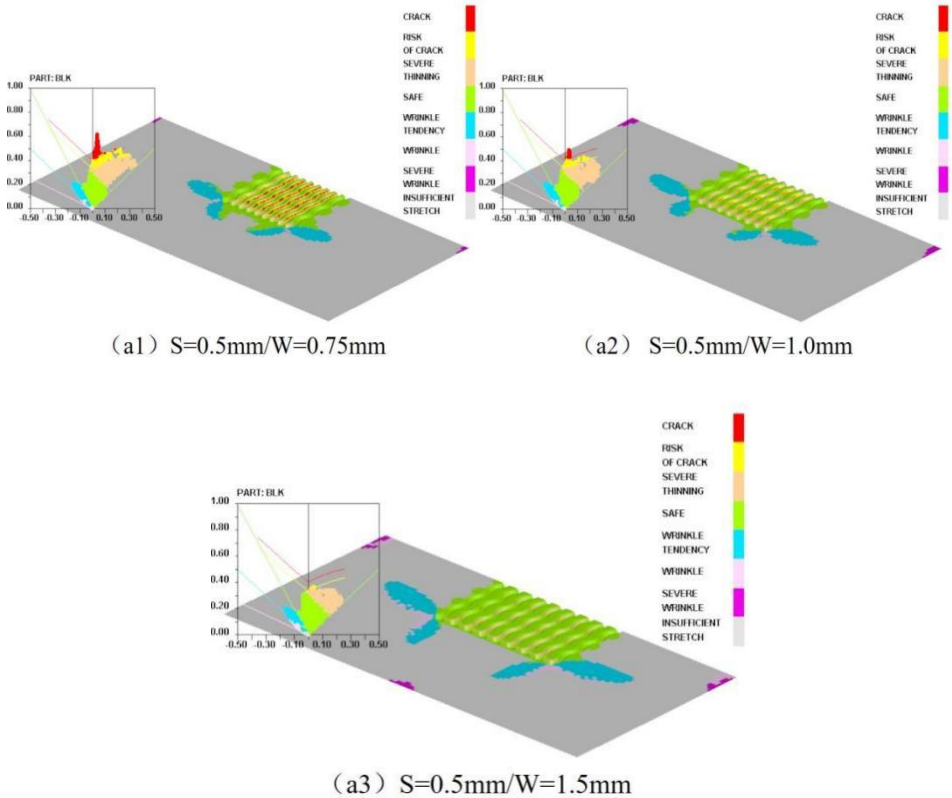

（a1）S=0.5mm/W=0.75mm　　（a2） S=0.5mm/W=1.0mm

（a3）S=0.5mm/W=1.5mm

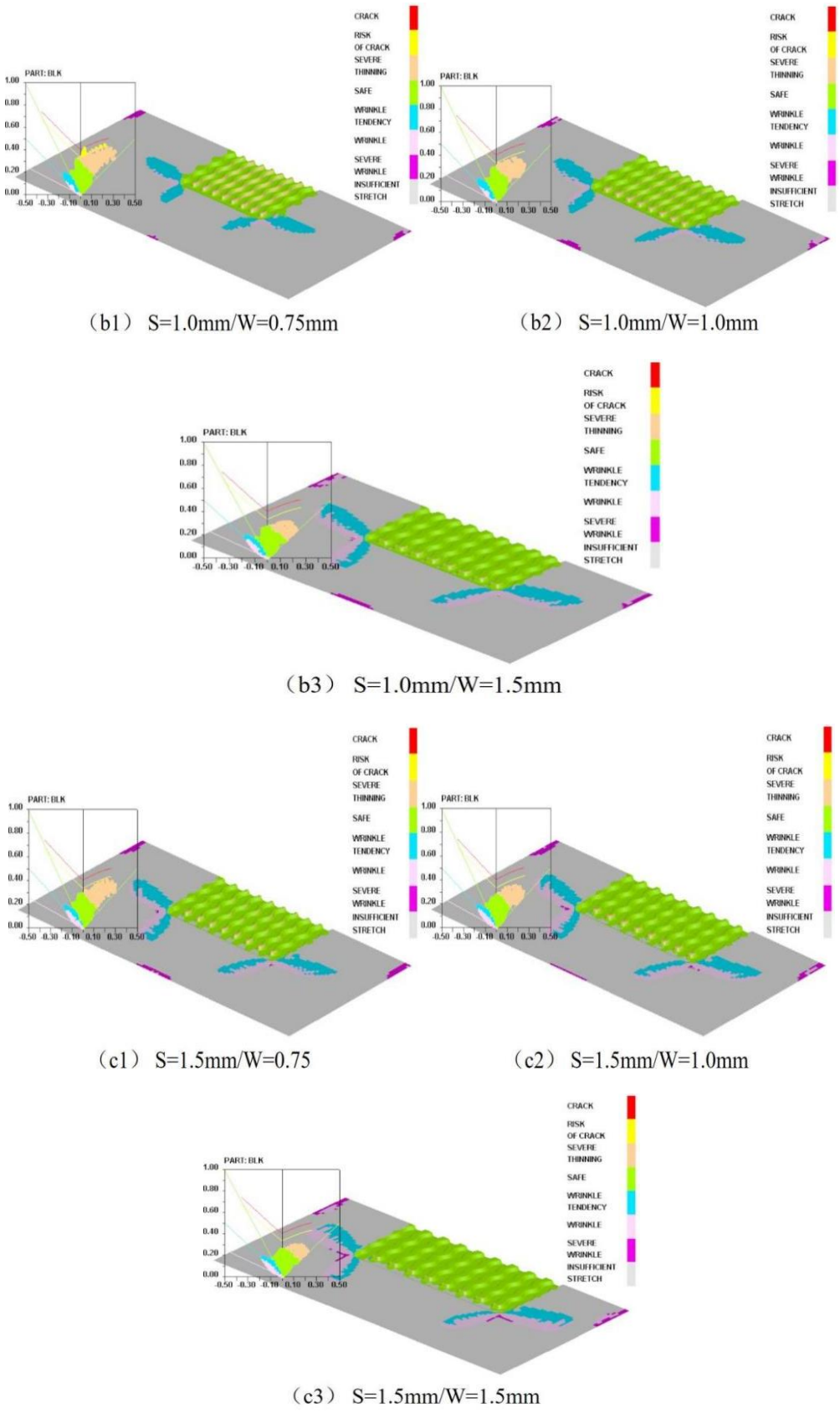

Fig. 7. Sheet forming limit diagram at different channel width and rib width combination

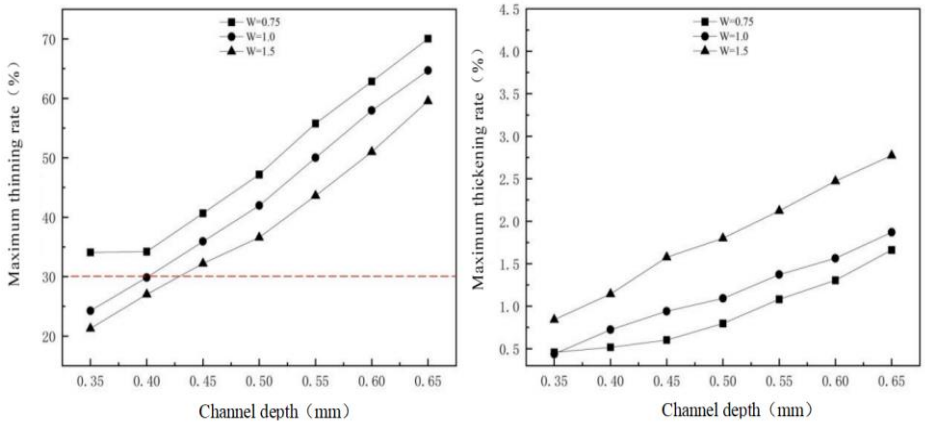

(a) S=0.5mm: maximum thinning rate and maximum thickening rate of sheet metal

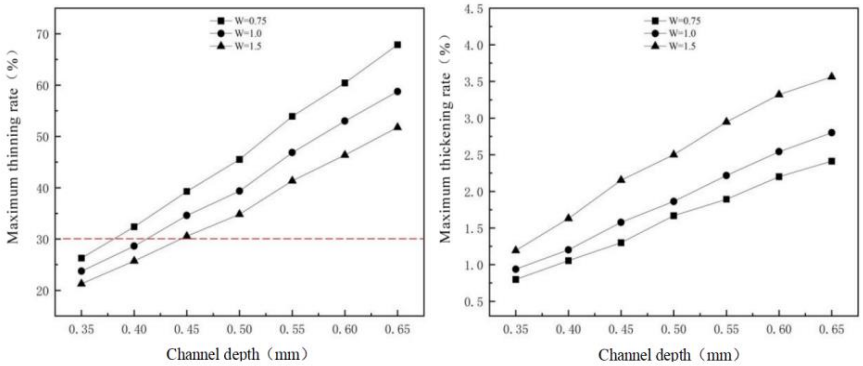

(b) S=1.0mm: maximum thinning rate and maximum thickening rate of sheet metal

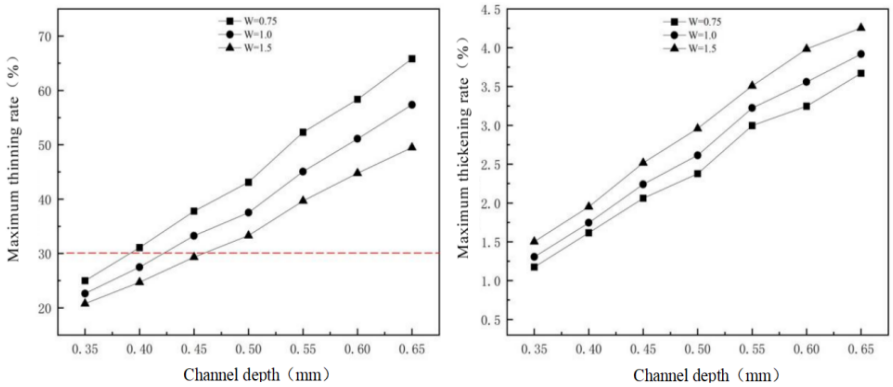

(c) S=1.5mm: maximum thinning rate and maximum thickening rate of sheet metal

Fig. 8. Simulation result at different channel width, rib width and forming depth combination

In Fig. 7, the parameter combination of (b3) :S=1.0mm, W=1.5, (c2) :S=1.5mm, W=1.0, (c3) :S=1.5mm, W=1.5mm, and the maximum thinning rate is 34.833%, 37.520% and 33.279%, respectively. Compared with (b3) and (c2), the rib width of (b3) is larger, the flow channel width is smaller, the minimum thinning rate is lower than (c2), and closer to the least thinning degree (c3), and this is true at all forming depths. Similarly, compared with (c2) in Fig. 7, the parameter combination of (a3) :S=0.5mm and W=1.5; the parameter combination of (c2)

:S=1.5mm and W=1.0mm; the rib width in (c2) is even greater than 0.5mm, but its maximum thinning rate is still higher than (c2). All these indicate that increasing the rib width has better effect on reducing the maximum thinning rate.

4.2 Thinning Optimization for the Corner Part of the Flow Channel

In order to keep the overall performance of the flow field unchanged to a certain extent and further reduce the thinning of the sidewall part of the flow channel corner, the rib height gradient structure is adopted on the basis of the rounded radius of Rw=0.75mm, and only the rib height of the flow channel corner is reduced. As shown in Fig. 9, H is the rib height of the original model, and a part of the rib is removed along the Y axis to reduce the rib height of the corner part. The section of the removed part perpendicular to the Y axis is a triangle, the height of the triangle is ΔH, and the area of the section remains unchanged, and the height of the remaining part of the rib gradually increases from left to right.

In the range of 0.225mm to 0.025mm, 9 groups of different ΔH were set respectively. Fig. 10 is the sheet metal forming limit diagram before and after optimization, and Fig. 11 is the corresponding thickness distribution cloud diagram. As shown in the figure, after optimization, the severe thinning of the whole board is greatly reduced and almost eliminated, and the thickness at the corner becomes more uniform. According to the maximum thinning rate curve of sheet metal in Fig. 12 (a), the maximum thinning rate of rotation Angle has not been improved in the range of Case1-Case4 (ΔH=0.225mm-0.15mm), which is less than 27.722% before optimization. In the range of Case5-Case9 (ΔH=0.1mm-0.025mm), the maximum thinning rate is reduced, and the highest is achieved when Case8 (ΔH=0.05mm), which can be reduced to 24.689% and the thickness reaches 0.752mm. The stress curve in Fig. 12 (b) shows that the maximum Von Mises stress value of the optimized plate first decreased and then increased, and the stress values of Case7 (ΔH=0.075mm) and Case8 (ΔH=0.05mm) were at the lowest level.

It can be seen that properly reducing the rib height of the corner can solve the stress concentration problem of the metal bipolar plate, and has a significant improvement effect on the thinning of the metal bipolar plate.

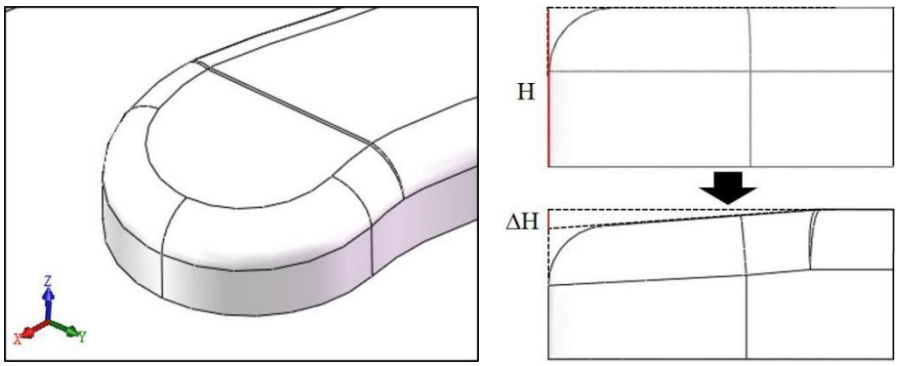

Fig. 9. Rib height gradient structure

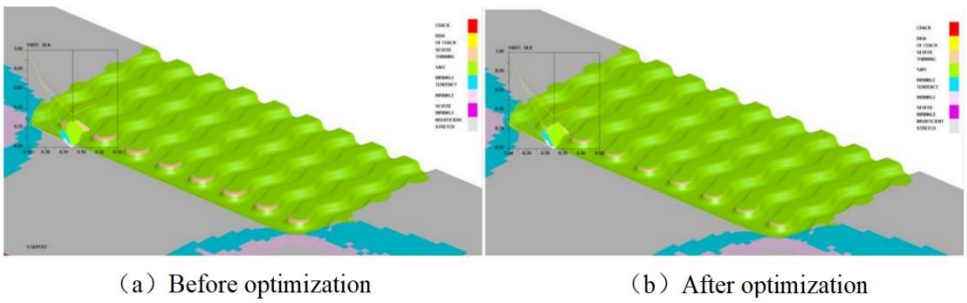

Fig. 10. Sheet forming limit diagram before and after optimization

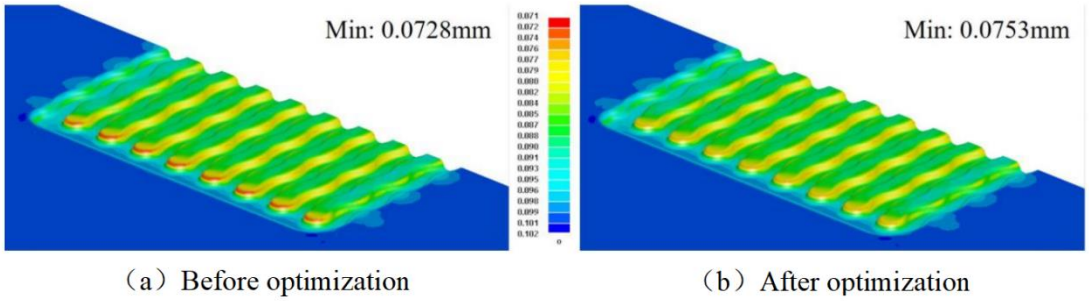

Fig. 11. Sheet thickness distribution before and after optimization

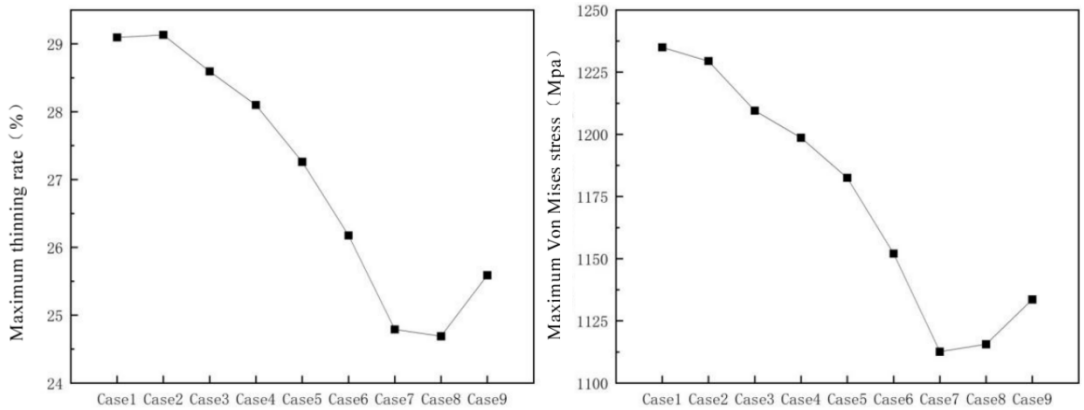

Fig. 12. Simulation result at different ΔH

4.3 Influence of Sine Curve Parameters of Wave Channel on Forming Quality

The wave channel in this paper is composed of sinusoidal curve y=Asin(ωx), in which parameter A is the amplitude, parameter ω controls the period size, and the greater the ω, the smaller the period. In this section, the period and amplitude of the sinusoidal curve of wave channel are taken as the research object, and the magnitude of the period and amplitude are controlled by changing parameters A and ω. 9 groups were set for both parameters: When studying parameter A, parameter ω=2 remained unchanged, and the setting range of parameter A was 0.05-0.45; When the parameter ω is studied, the parameter A=0.25 remains unchanged, and the study range of parameter ω is 0.5-4.5. Other structural parameters follow the optimized model.

4.3.1 Influence of different A values on forming quality

Fig. 13 shows the sheet metal forming limit diagram under different values of A, and Fig. 14 shows the corresponding thickness distribution cloud diagram. As shown in the figure, the severe thinning amount of the whole plate increases with the increase of parameter A, and the thickness of the largest part of the amplitude of the sine curve gradually approaches the thickness of the corner part of the flow channel and begins to produce serious thinning. With the increase of parameter A, the wrinkling amount of the whole plate slightly decreases, and the wrinkling at the corner of the edge of the flow field is weakened. It can be seen that when the value of parameter A reaches 0.35, the severe wrinkling unit at the corner of the edge of the flow field completely disappears, and the structures (2) and (3) marked by the red dashed line in Fig. 14 are shown.

The ribs in the structure (2) protrude outwards, and the thickness of the rounded corners of the die is the smallest. In the thickness distribution cloud map, it can be seen that the minimum thickness at structure (2) is closer to the minimum thickness of the flow channel Angle. The ribs in the structure (3) are concave inward, and the thickness of the rounded corners of the punch is the smallest. When the A value is large

enough, it can be found that both structure (2) and structure (3) have severely thinned elements. Fig. 15 shows the cloud diagram of stress distribution of sheet metal when A=0.45. It can be seen that in addition to the corner of the flow channel, the part of the sinusoidal curve with the largest value also produces stress concentration.

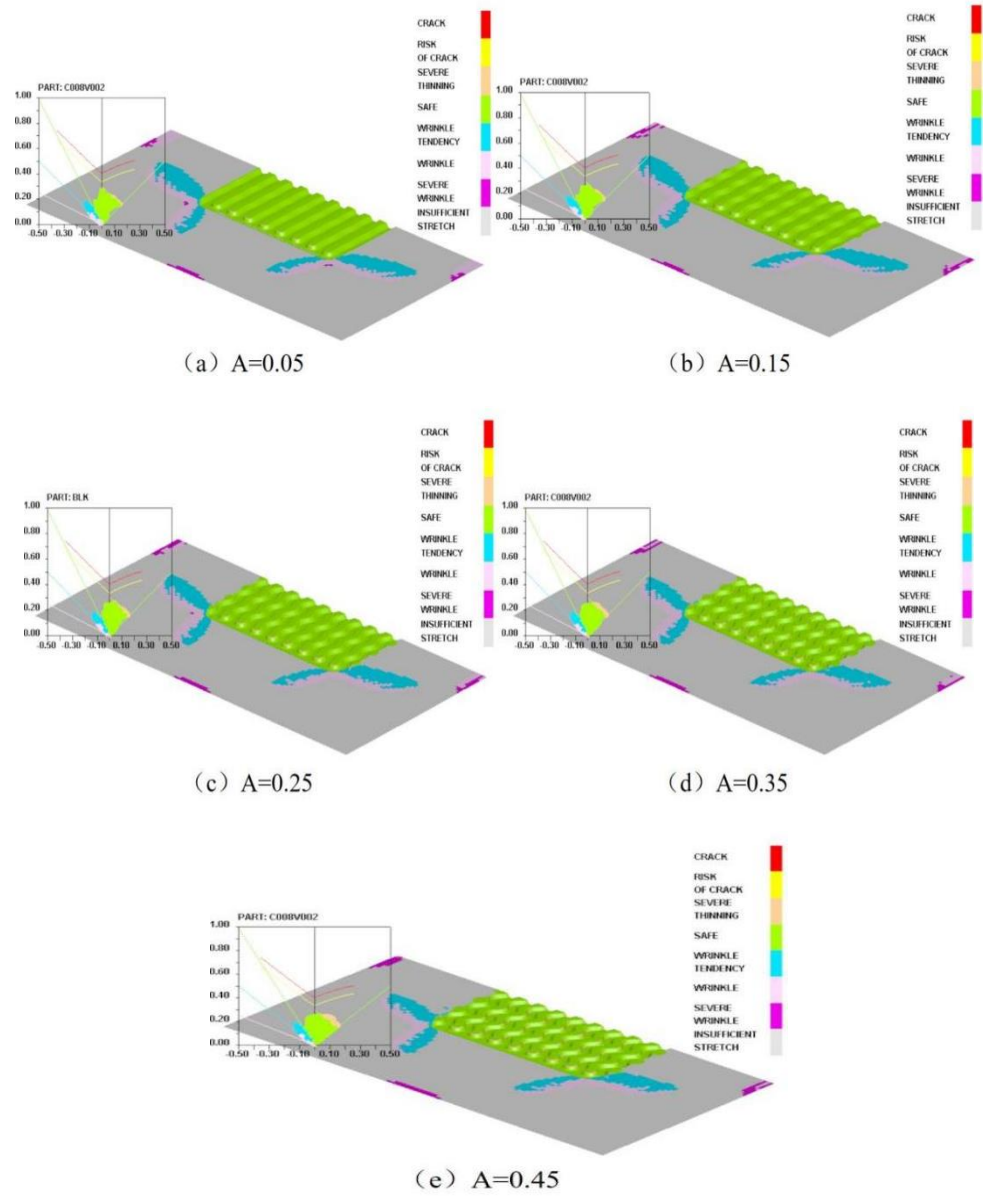

Fig. 13. Sheet forming limit diagram at different A

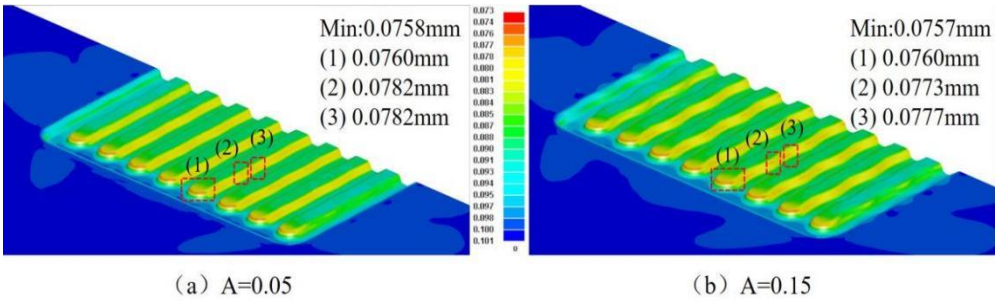

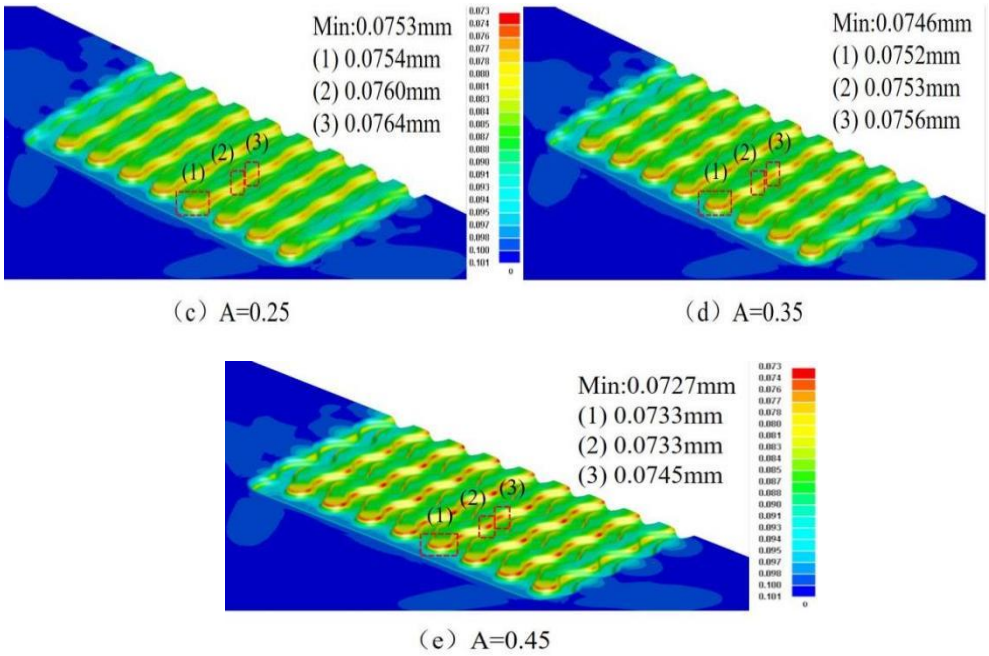

Fig. 14. Sheet thickness distribution at different A

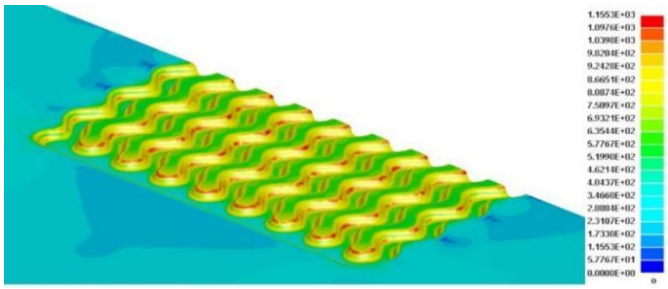

Fig. 15. The sheet von mises stress distribution at A=0.45

In Fig. 16 (a), the maximum thinning rate of metal bipolar plate increases with the increase of parameter A, and the increase from 0.05 to 0.3 is small, ranging from 24.162% to 24.847%, the difference is only 0.685%, and the increase from 0.3 to 0.45 is large. From 24.847% to 27.325%, the difference is 2.478%, and the difference between the maximum and minimum of the curve is 3.163%. In Fig. 16 (b) sheet metal stress curve, the maximum Von Mises stress value showed A general upward trend with the increase of parameter A, and began to surge before and after A was 0.3. Fig. 16 (c) shows the curve of the maximum thickening rate of sheet metal. It shows that the curve of the maximum thickening rate generally presents a downward trend, with the maximum value being 1.281% and the minimum value being 0.981%, and the difference is only 0.3%.

According to the above analysis, under the simulated conditions, the increase of A value will increase the maximum Von Mises stress value of the metal bipolar plate, resulting in greater thinning amount. At this time, stress concentration occurs not only in the corner of the flow channel, but also in the maximum sinusoidal amplitude of the wave flow channel, and begins to produce serious thinning. In addition, the minimum thickness of the plates in these two parts will gradually approach with the increase of the A value, while the maximum thickness increase rate and wrinkling amount will slightly decrease.

4.3.2 Influence of different ω values on forming quality

The amplitude is changed by adjusting the size of the parameter ω, the larger the parameter ω,

the smaller the period. Fig. 17 shows the sheet metal forming limit diagram under different ω values, and Fig. 18 shows the corresponding thickness distribution cloud diagram. With the increase of ω, a large number of severely thinned areas are produced, and the amount of wrinkling will gradually decrease. As shown in Fig. 18 (e) sheet metal thickness distribution diagram, when ω=4.5, the thickness at the maximum value point has been completely lower than the corner area.

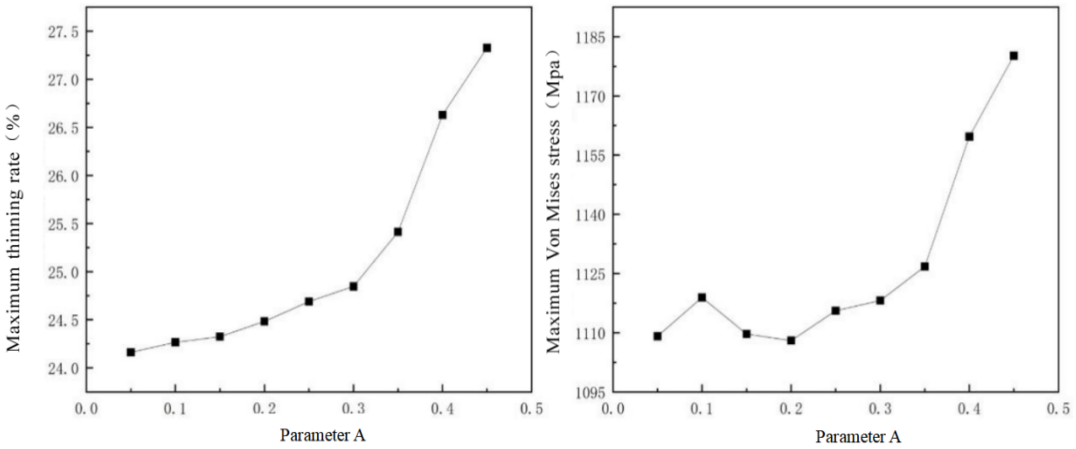

(a) Maximum thinning rate of sheet metal (b) Maximum V on Mises stress of sheet metal

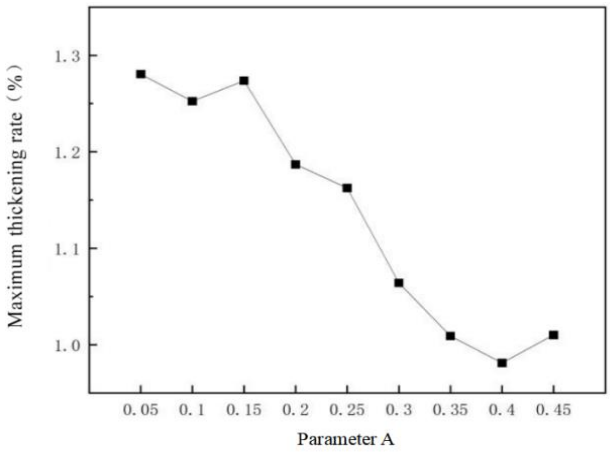

(c) maximum thickness increase of sheet metal

Fig. 16. Simulation result at different A

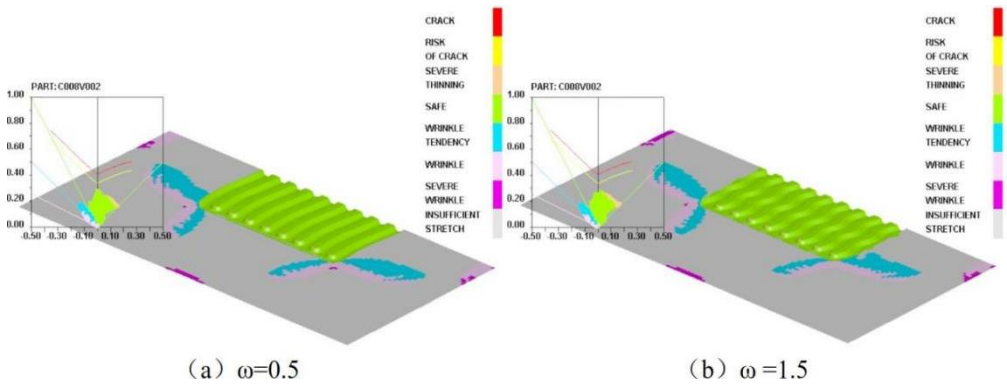

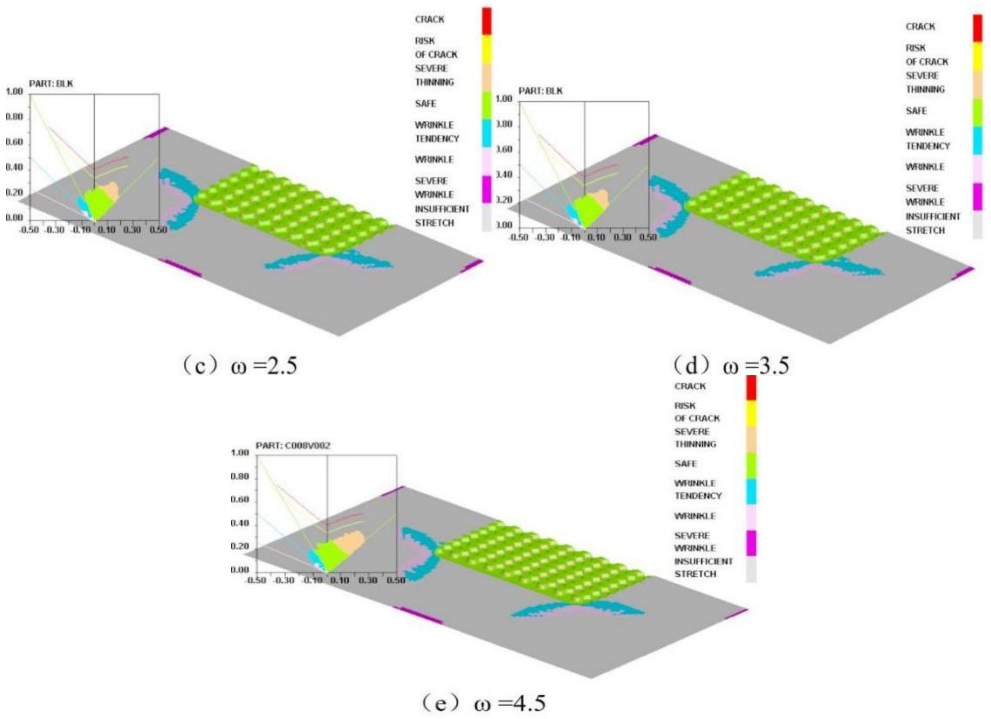

Fig. 17. Sheet forming limit diagram at different ω

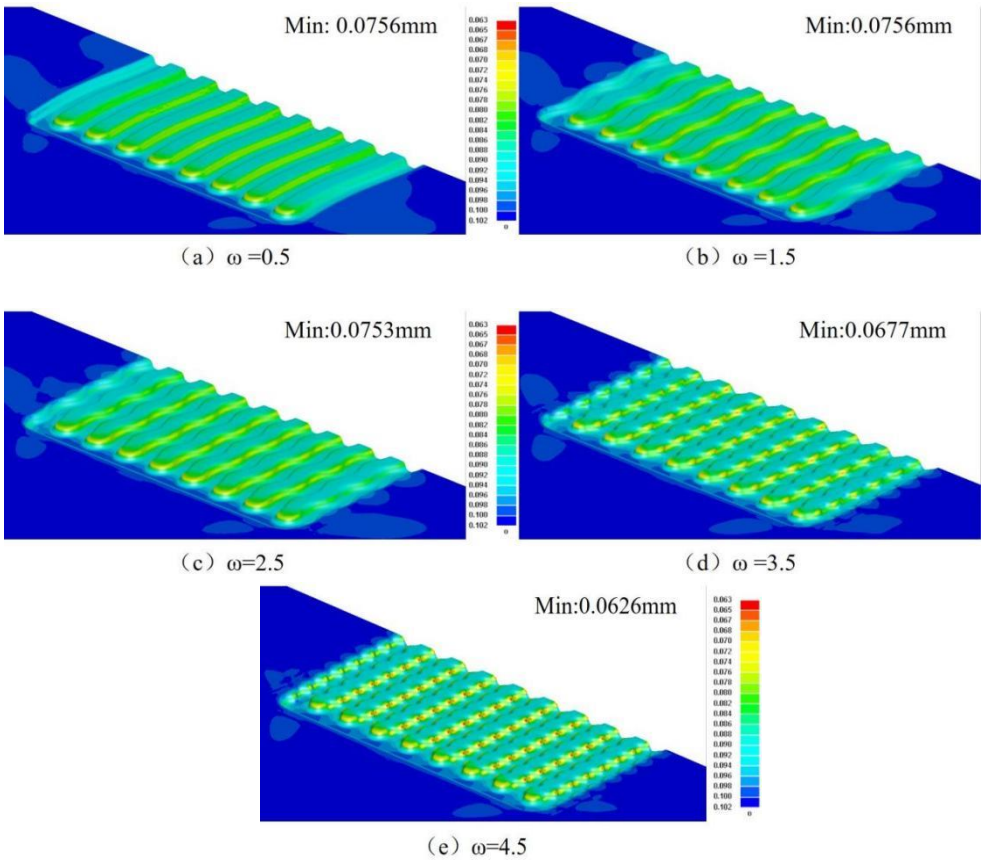

Fig. 18. Sheet thickness distribution at different ω

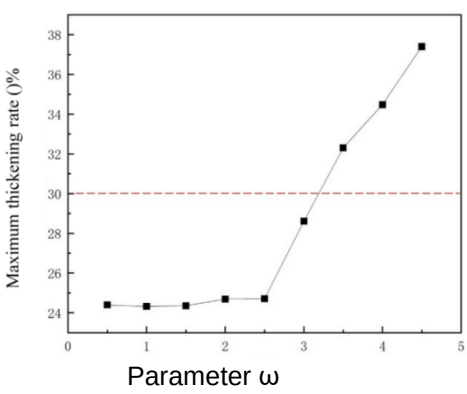

(a) Maximum thinning rate of sheet metal

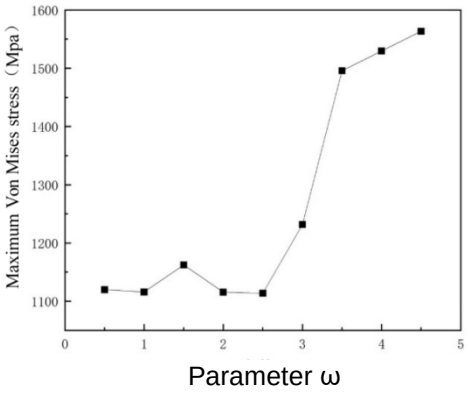

(b) Maximum Von Mises stress of sheet metal

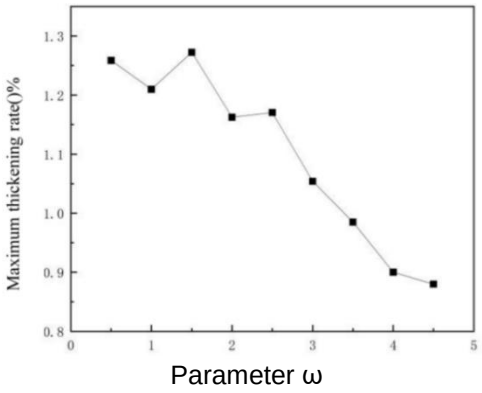

(c) maximum thickness increase of sheet metal

Fig. 19. Simulation result at different ω

According to the maximum thinning rate curve of sheet metal in Fig. 19 (a), the maximum thinning rate of metal bipolar plate hardly changes between ω=0.5-2.5, rapidly rises between ω=2.5-4.5, and exceeds 30% when ω reaches 3.5, and its maximum and minimum values are 37.403% and 24.395%, respectively. The difference is 13.008%. In the sheet metal stress curve shown in Fig. 19 (b), the maximum VonMises stress value showed A general upward trend with the increase of ω, and the change was similar to parameter A. Fig. 19 (c) shows the curve of maximum thickening rate of sheet metal. It can be seen that the curve shows a downward trend before 3.5. When ω=3.5, the maximum thickening rate reaches the minimum value of 0.985%, and then starts to rise after 3.5, with the difference between the maximum and the minimum value only 0.341%.

It can be seen from the above analysis that under the simulated conditions, increasing the ω value will only reduce the wrinkle amount slightly, and mainly increase the number and degree of severely thinning areas in the metal bipolar plate, which is not conducive to the forming of the metal bipolar plate.

5. CONCLUSION

In this paper, the effects of channel section profile dimensions (channel width, rib width, forming depth) and channel plane profile dimensions (sine curve parameters A, ω) on the forming quality of the metal bipolar plate in wave flow field are studied, and the severely thinned structures in the metal bipolar plate are optimized. The formability of metal bipolar plate with wave flow field structure was verified and investigated. The results show that:

(1) The lower forming depth is conducive to eliminating thinning and wrinkling. Larger channel width and rib width are beneficial to alleviate the thinning of metal bipolar plate, especially the effect of increasing the rib width is better. Compared with increasing the channel width and rib width at the same time, the

difference in thinning degree between the relatively small channel width and the relatively large rib width is smaller, but the maximum thickening rate is lower and the wrinkling is less. In general, the forming quality of the bipolar plate is better when the width of the runner is S=1.0mm, the width of the rib is W=1.5mm and the forming depth is H=0.5mm.

(2) When the rib height of the corner part is reduced, the maximum thinning rate can be reduced from the original 34.833% to the minimum to 24.689% and the thickness can reach 0.0753mm when the channel width S=1.0mm, the rib width W=1.5mm and the forming depth H=0.5mm. It can significantly improve the thinning problem caused by stress concentration in the corner part.

(3) The results show that the larger parameters A and ω will lead to the increase of the thinning amount and the lower change of the wrinkle amount. With the increase of A value and ω, the stress will gradually concentrate at the maximum amplitude of the sinusoidal curve, resulting in serious thinning, increasing the risk of rupture, which is not conducive to forming.

COMPETING INTERESTS

Authors have declared that no competing interests exist.

REFERENCES

1. Pei PH, Meng YN, Chen DF, Ren P, Wang MK, Wang XZ. Lifetime prediction method of proton exchange membrane fuel cells based on current degradation law. Energy. 2023;265:126341.
2. Huang Y, Song JN, Deng XY, Chen S, Zhang X, Ma ZP, Chen LJ, Wu YL. Numerical investigation of baffle shape effects on performance and mass transfer of proton exchange membrane fuel cell. Energy. 2023;266:126448.
3. Xing L, Chang HW, Zhu RQ, Wang T, Zou QF, Xiang WT, Tu ZK. Thermal analysis and management of proton exchange membrane fuel cell stacks for automotive vehicle. Int J Hydrogen Energ. 2021;46: 32665-32675.
4. Li YH, Pei PC, Ma Z, Ren P, Wu ZY, Chen DF, Huang H. Characteristic analysis in lowering current density based on pressure drop for avoiding flooding in proton exchange membrane fuel cell. Appl Energ. 2019;248:321-329.
5. Lu HX, Chen J, Yan CZ, Liu H. On-line fault diagnosis for proton exchange membrane fuel cells based on a fast electrochemical impedance spectroscopy measurement. J Power Sources. 2019;430:233-243.
6. De-Troya JJ, Alvarez C, Fernandez-Garrido C, Carral L. Analysing the possibilities of using fuel cells in ships. Int J Hydrogen Energ. 2016;41:2853-2866.
7. Pourrahmani H, Gay M, Herle JV. Electric vehicle charging station using fuel cell technology: Two different scenarios and thermodynamic analysis. Energy Rep. 2021;7:6955-6972.
8. Qin fei, Guo pengyan. Research status of hydrogen fuel cell stack packaging[J]. Automotive electrical appliance. 2022(3):14-17.
9. Simon T. Thompson, Brian D. James, Jennie M, et al. Direct hydrogen fuel cell electric vehicle cost analysis: System and high-volume manufacturing description, validation, and outlook[J]. Journal of Power Sources. 2018;399:304-313.
10. Guo H, Wang MH, Liu JX, Nie ZH, Ye F, Ma CF. Temperature distribution on anodic surface of membrane electrode assembly in proton exchange membrane fuel cell with interdigitated flow bed. J Power Sources. 2015;273:775-783.
11. Shen J, Tu ZK, Chan SH. Performance enhancement in a proton exchange membrane fuel cell with a novel 3D flow field. Appl Therm Eng. 2020;164:114464.
12. Jang JY, Cheng CH, Liao WT, Huang YX, Tsai YC. Experimental and numerical study of proton exchange membrane fuel cell with spiral flow channels. Appl. Energy. 2012;99:67–79.
13. Tsung-Chia Chen, Jiun-Ming Ye. A micro-stamping process analysis of metallic bipolar plates channel[C]. //2011 IEEE International Conference on Nano/Micro Engineered and Molecular Systems. [v.1].: IEEE. 2011:597-602.
14. Zhai hua, Li yuan, Shi wenchao, el. Research on thickness thinning of metal bipolar plate in corner area of stamped PEMFC serpentine runner[J]. Journal of plastic engineering. 2021; 28(02):22-28.
15. Kivanc Karacan, Selahattin Celik, Serkan Toros, et al. Investigation of formability of metallic bipolar plates via stamping for light-weight PEM fuel cells[J]. International

Journal of Hydrogen Energy. 2020;45(60): 35149-35161.
16. Zhang lili, Wang kaikun. Numerical simulation and experiment of stamping and forming of PEMFC metal bipolar plate[J].Precision forming engineering. 2017;9(06):163-169.
17. Peng SW, Wu HW. A three-dimensional numerical investigation of trapezoid baffles effect on non-isothermal reactant transport and cell net power in a PEMFC. Appl Energ. 2015;143:81-95.
18. Xia L, Yu ZT, Xu GP, Ji SB, Sun B. Design and optimization of a novel composite bionic flow field structure using three-dimensional multiphase computational fluid dynamic method for proton exchange membrane fuel cell. Energ Convers Manage. 2021;247:114707.
19. Liu Z, Zeng X, Ge Y, Shen J, Liu W. Multi-objective optimization of operating conditions and channel structure for a proton exchange membrane fuel cell. Int J Heat Mass Tran. 2017;111:289–98.
20. Maharudrayya S, Jayanti S, Deshpande AP. Pressure drop and flow distribution in multiple parallel-channel configurations used in proton-exchange membrane fuel cell stacks. J Power Sources. 2006; 157(1):358–67.

Peer-review history:
The peer review history for this paper can be accessed here:
https://www.sdiarticle5.com/review-history/111352